available at www.sciencedirect.com
journal homepage: www.eu-openscience.europeanurology.com

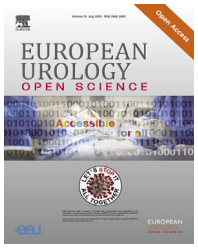

European Association of Urology

Prostate Cancer

Analysis of Prostate Cancer Tumor Microenvironment Identifies Reduced Stromal CD4 Effector T-cell Infiltration in Tumors with Pelvic Nodal Metastasis

Chara Ntala [a,b], *Mark Salji* [a,b], *Jonathan Salmond* [c], *Leah Officer* [a,d], *Ana Vieira Teodosio* [d], *Arnaud Blomme* [a], *Ewan J. McGhee* [a], *Ian Powley* [a,e], *Imran Ahmad* [a,b], *Marianna Kruithof-de Julio* [f], *George Thalmann* [f], *Ed Roberts* [a], *Carl S. Goodyear* [g], *Tamara Jamaspishvili* [h], *David M. Berman* [h], *Leo M. Carlin* [a,b], *John Le Quesne* [b,d,e], *Hing Y. Leung* [a,b,*]

[a] *CRUK Beatson Institute, Glasgow, UK;* [b] *Institute of Cancer Sciences, University of Glasgow, Garscube Estate, Switchback Road, Glasgow, UK;* [c] *Department of Pathology, Queen Elizabeth University Hospital, Glasgow, UK;* [d] *Medical Research Council Toxicology Unit, University of Cambridge, Leicester, UK;* [e] *Leicester Cancer Research Centre, University of Leicester, Leicester, UK;* [f] *Department of Urology, Bern University Hospital, University of Bern, Bern, Switzerland;* [g] *Institute of Infection, Immunity and Inflammation, University of Glasgow, Glasgow, UK;* [h] *Department of Pathology and Molecular Medicine, Queen's University, Kingston, ON, Canada*

Article info

Article history:
Accepted May 5, 2021

Associate Editor:
Guillaume Ploussard

Keywords:
Prostate cancer
Tumor microenvironment
Immune cells
Lymph node

Abstract

Background: Pelvic nodal metastasis in prostate cancer impacts patient outcome negatively.
Objective: To explore tumor-infiltrating immune cells as a potential predictive tool for regional lymph node (LN) metastasis.
Design, setting, and participants: We applied multiplex immunofluorescence and targeted transcriptomic analysis on 94 radical prostatectomy specimens in patients with (LN+) or without (LN–) pelvic nodal metastases. Both intraepithelial and stromal infiltrations of immune cells and differentially expressed genes (mRNA and protein levels) were correlated with the nodal status.
Outcome measurements and statistical analysis: The identified CD4 effector cell signature of nodal metastasis was validated in a comparable independent patient cohort of 184 informative cases. Patient outcome analysis and decision curve analysis were performed with the CD4 effector cell density–based signature.
Results and limitations: In the discovery cohort, both tumor epithelium and stroma from patients with nodal metastasis had significantly lower infiltration of multiple immune cell types, with stromal CD4 effector cells highlighted as the top candidate marker. Targeted gene expression analysis and confirmatory protein analysis revealed key alteration of extracellular matrix components in tumors with nodal metastasis. Of note, stromal CD4 immune cell density was a significant

* Corresponding author. CRUK Beatson Institute, Garscube Estate, Switchback Road, Glasgow, G61 1BD, UK; Institute of Cancer Sciences, University of Glasgow, Garscube Estate, Switchback Road, Glasgow, G61 1QH, UK. Tel. +44 141 330 3658.
E-mail address: h.leung@beatson.gla.ac.uk (H.Y. Leung).

http://dx.doi.org/10.1016/j.euros.2021.05.001

independent predictor of LN metastasis (odds ratio [OR] = 0.15, $p = 0.004$), and was further validated as a significant predictor of nodal metastasis in the validation cohort (OR = 0.26, $p < 0.001$).

Conclusions: Decreased T-cell infiltrates in the primary tumor (particularly CD4 effector cells) are associated with a higher risk of LN metastasis. Future evaluation of CD4-based assays on prostate cancer diagnostic biopsy materials may improve selection of at-risk patients for the treatment of LN metastasis.

Patient summary: In this report, we found that cancer showing evidence of cancer metastasis to the lymph nodes tends to have less immune cells present within the tumor. We conclude that the extent of immune cells present within a prostate tumor can help doctors determine the most appropriate treatment plan for individual patients.

1. Introduction

Prostate cancer (PCa) is the second most prevalent cancer in men worldwide [1]. During PCa progression, regional lymph nodes (LNs) are common sites for metastases. Even with the adoption of the Briganti nomogram and similar strategies, only around 20% of patients undergoing extended pelvic node dissection will be confirmed to have histological evidence of nodal metastasis. There is a lack of sensitive and specific markers for predicting cancer spread to the LNs at the time of diagnosis.

Tumor-infiltrating immune cells have previously been identified as prognostic and predictive biomarkers in several cancers [2–7]. The exact immune cell subpopulation, and its functional polarization and spatial distribution have been shown to influence cancer aggressiveness, metastatic potential, and clinical outcome for cancer patients [4,5,8]. Therefore, the *in situ* cancer immune cell composition may have direct clinical implications for prognosis as well as therapeutic responses.

Multiplex immunofluorescence (mIF) has been instrumental in the investigation of the tumor microenvironment. Fluorescent signals are easily quantifiable due to their linear and additive nature, allowing for more objective and reproducible quantitation compared with chromogenic immunohistochemistry (IHC) [9]. The benefits of multiplexing with tyramide signal amplification lie in collecting maximum information from a single tissue section [10]. Therefore, cell populations can be classified accurately, and their spatial associations and frequency of coexpression among different cell types can be determined [4,11].

The reported relationships between tumor-infiltrating immune cells in PCa with patient outcomes have varied widely in the literature. Several studies have associated different immune cells, such as macrophages, and CD8 and CD4 T lymphocytes, with PCa patient survival; however, these results have been inconsistent [12–16]. Therefore, it is essential to study the baseline immune status of high-risk disease in order to gain a better understanding of disease progression and to inform treatment plans. In this study, we hypothesized that a local immune cell signature can predict pelvic nodal metastasis. We further investigated for potential correlation between tumoral immune infiltrates and common genetic alterations in PCa, such as *ERG* translocation and loss of PTEN expression.

We characterized the tumor immune infiltrates within radical prostatectomy (RP) specimens by mIF, along with targeted transcriptomic analysis of the tumor microenvironment. We identified a CD4 effector cell–based tumoral immune signature of LN+ disease, which was then validated in a comparable independent patient cohort. Together, we explored the possibility of exploiting the immune landscape of intermediate- and high-risk PCa as potential prognostic markers for nodal metastasis.

2. Patients and methods

2.1. Discovery cohort

Formalin-fixed, paraffin-embedded (FFPE) histological sections from intermediate- and high-risk PCa patients who underwent RP and lymphadenectomy with curative intent (50 with and 45 without LN metastasis) were retrospectively identified between June 04, 2008, and January 23, 2018, at Queen Elizabeth University Hospital in Glasgow. All patients found positive for pelvic node following RP and pelvic node dissection in this period were selected for an analysis. A similar number of patients with similar clinicopathological factors but negative for pelvic nodes following surgery were then included as controls.

2.2. Validation cohort

To validate findings from the discovery cohort, we studied a tissue microarray (TMA) of RP specimens containing primary PCa from University of Bern. This included 285 patients with primary PCa who underwent RP. A total of 251 patients had one 0.6 μm core and 34 patients had two 0.6 μm cores from the PCa index lesion. Data from 184 cases were informative with adequate cancer content in the tissue samples and interpretable images following staining.

2.3. Laboratory investigations

Methodologies for the following are provided in the Supplementary material:

1 Construction of a TMA
2 Multiplex immunofluorescence staining

3 Machine learning and multispectral analysis (Supplementary Fig. 1)
4 Transcriptomic analysis of FFPE tissue using HTG EdgeSeq Precision Immuno-Oncology Panel (Supplementary Table 1)
5 Manual chromogenic IHC and scoring
6 Second harmonic generation (SHG) image acquisition and analysis for the determination of collagen quantity and quality

2.4. Statistical methods

Statistical analyses were carried out with Graph Prism 8 and IBM SPSS statistics 25. R v3.5.2 software was used for creating CD4 effector T-cell density plots, survival analysis, receiver operator characteristic (ROC) analysis, and decision curve analysis. Comparisons between groups were conducted using Mann–Whitney U tests (unpaired, nonparametric, two tailed), and Fisher's and chi-square tests where appropriate. Kaplan-Meier curves were compared using Cox's proportional hazards regression model. ROC curve analysis and multivariate logistic regression models were used to identify predictive factors of LN metastasis. For the targeted gene expression panel, HTG reveal software was used for statistical analysis using the DESeq2 test with an adjusted p value of <0.05 and a log fold change value of >1.5.

3. Results

3.1. Clinicopathological characteristics

Patient clinicopathological characteristics included in the discovery TMA are presented in Table 1. Besides their age, patients with and without LN metastasis (LN+, n = 50 and LN–, n = 44, respectively) have highly comparable clinicopathological parameters (including the number of excised LNs, preoperative prostate-specific antigen [PSA] levels, pT stage, Gleason score, and presence of perineural invasion).

3.2. Tumoral immune infiltrates are associated with pelvic nodal disease

We developed two mIF protocols, which allowed for the simultaneous evaluation of up to six markers in a single FFPE tissue section (Figs. 1 and 2). Each tissue core was visually examined, and cores with benign tissue, tissue folding, or staining artifacts were excluded. The immune cell densities were quantified within the epithelial and stromal compartments separately.

Tumors with LN metastasis generally had less immune infiltration (Table 2 and Fig. 3), with significant reduced tumor (both intraepithelial and stromal) infiltration by M1-like macrophages and CD8 effector T cells. Of particular interest, stromal CD4 effector T-cell infiltration showed a large difference between LN– and LN+ tumors: 32.5 versus 91.35 cells/mm^2 ($p < 0.001$; Table 2). There were no significant differences in M2-like macrophages, B cells, CD4 regulatory T cells, CD8 regulatory T cells, CD4 PD-1–positive T cells, and CD8 PD-1–positive T cells between patients with or without LN involvement.

3.3. Common molecular changes in PCa did not correlate with immune cell densities

Of the 94 patients in our TMA, 92, 91, and 89 had at least two out of three evaluable cores for ERG, PTEN, and Ki67 staining by IHC, respectively (Supplementary Table 2 and Supplementary Fig. 2). Consistent with the reported incidence of TMPRSS2/ERG translocation [17,18], 43/92 (47%) stained positive for ERG. However, ERG immunoreactivity did not correlate with nodal metastasis (p = 0.836). PTEN staining was detected in 52/91 (57%) patients. Consistent with previous reports [19,20], with PTEN loss significantly associated with nodal metastasis ($p < 0.001$). Overall, immune cell infiltrates did not correlate with ERG status, PTEN status, or proliferation index (Ki67 staining; Supplementary Tables 3–5).

3.4. Transcriptomic analysis highlighted the association between altered tumor extracellular matrix and nodal status

To gain additional insight into the molecular mechanisms associated with LN+ prostate tumors, we used a targeted HTG EdgeSeq Immuno-Oncology panel (Supplementary Table 1) to compare LN+ versus LN– prostate tumors.

Table 1 – Clinical and histopathological characteristics of the discovery TMA of patients with (LN+) and without (LN–) lymph node metastasis

	Overall	Lymph node metastasis		
	N = 94	LN–, n = 44	LN+, n = 50	p value
Age at diagnosis, median (95% CI)	65 (63–66)	67 (66–70)	62 (59–65)	<0.001
Number of lymph nodes excised, median (95% CI)	15 (13–17)	17 (14–18)	13.5 (10–17)	0.051
Peak PSA, median (95% CI)	14.8 (12.3–16.7)	15.5 (11.5–17.7)	14.2 (11–17)	0.831
Stage, N (%)				0.089
pT2	34 (36.17)	20 (45.45)	14 (28)	
pT3-T4	60 (63.83)	24 (54.55)	36 (72)	
Gleason score, N (%)				0.109
7	65 (69.15)	34 (77.27)	31 (62)	
>7 (8–9)	29 (30.85)	10 (22.73)	19 (38)	
PNI, N (%)				0.156
Negative	15 (15.96)	10 (22.73)	5 (10)	
Positive	79 (84.04)	34 (77.27)	45 (90)	
Relapse-free survival, median (95% CI)	39 (44.3–33.6)	39 (53.9–41.5)	40 (57.1–39.8)	0.404

CI = confidence interval; LN = lymph node; PNI = perineural invasion; PSA = prostate-specific antigen; TMA = tissue microarray.
Mann-Whitney and Fisher's exact tests were used for statistical calculations.

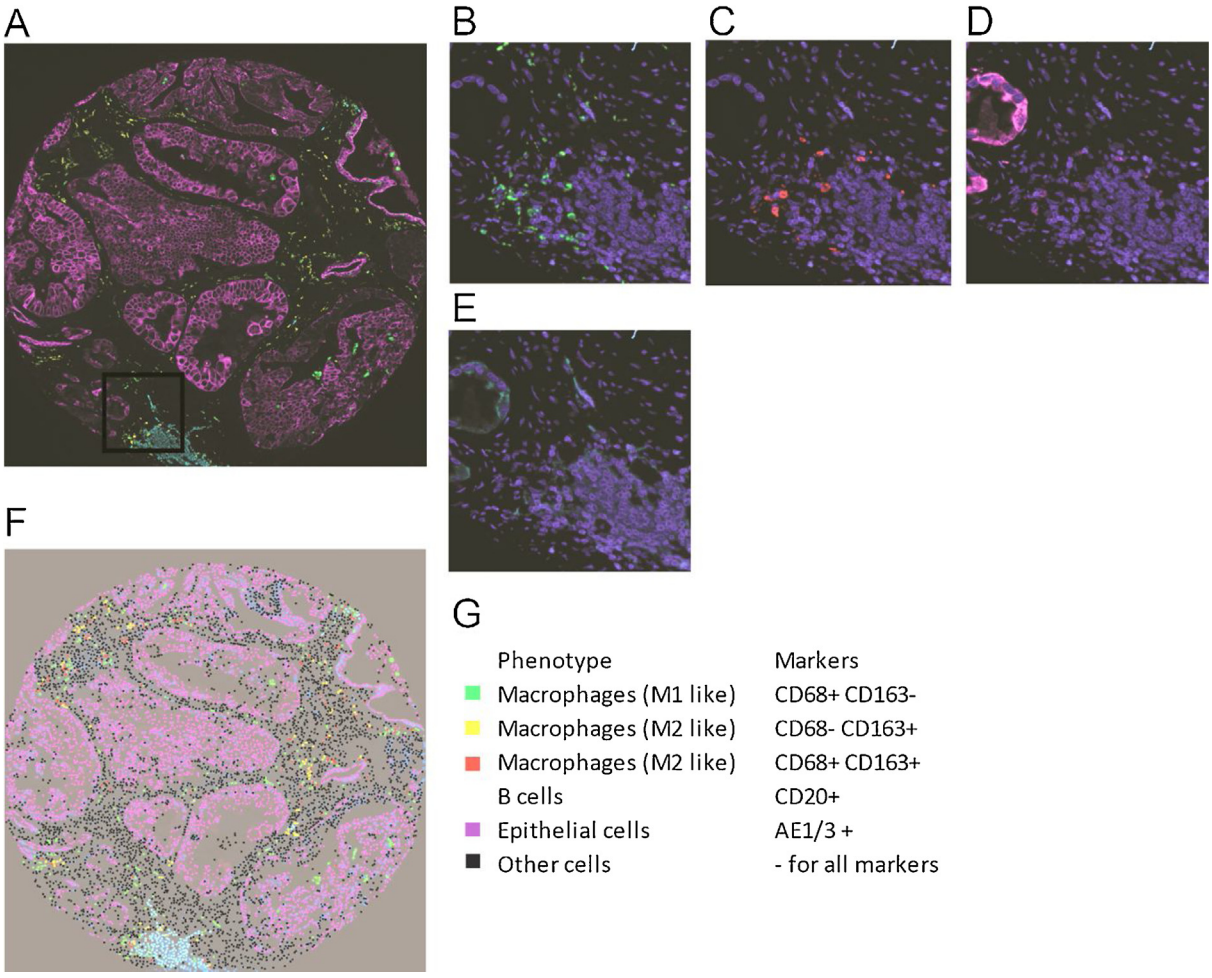

Fig. 1 – Application of a macrophage and B-cell multiplex immunofluorescence panel in prostate cancer primary tumors. (A) A spectrally unmixed prostate cancer core stained with the macrophage and B-cell panel (panel 1). Enlarged subsections of the core highlighted in Figure 1A, showing each markers of the composite image individually after spectral unmixing, together with DAPI nuclear marker (blue pseudocolor) and autofluorescence signal (black pseudocolor): (B) CD68 (labeled with Opal 520, green pseudocolor), (C) CD163 (labeled with Opal 570, red pseudocolor), (D) AE1/3 Pancytokeratin (labeled with Opal 650, magenta pseudocolor), (E) CD20 (labeled with Opal 690, cyan pseudocolor), and (F) cell phenotype map of the same core as in Figure 1A identifying the cell populations defined by the individual markers of the multiplex immunofluorescence stain. (G) Summary of each defined cell phenotype (pseudocolor used for visualization and associated markers). (Images shown were obtained at 10× magnification.)

Nineteen genes were identified to be differentially expressed: 15 were upregulated and four were down-regulated in LN+ cases (DESeq2, adjusted $p < 0.05$, fold change >1.5; Fig. 4A). Interestingly, among the most upregulated genes in LN+ cases were extracellular matrix (ECM) core proteins, namely, collagen type I and III (*COL1A1* and *COL3A1*) and fibronectin 1 (*FN1*; Fig. 4A). We applied IHC to study protein expression of collagen I, collagen III, and FN1. In addition, we characterized the collagen structure by SHG multiphoton microscopy (without the use of antibodies). Gray level co-occurrence matrix (GLCM) texture analysis was used to compare the SHG images. The collagen score derived from the mean decay distance of the SHG signal showed that the structure of collagen I was significantly associated with LN spread: 17.72 (interquartile range [IQR] 11.52–34) in LN+ versus 13.43 (IQR 9.14–21.46) in LN– ($p < 0.001$; Fig. 4B). In contrast to the findings regarding the collagen structure, collagen I staining (assaying for its level) within the stroma did not show any statistically significant differences between the two groups: 32.92 (95% confidence interval [CI] 29.89–21.8) in LN+ versus 29.87 (95% CI 21.8–37.49) in LN– ($p = 0.189$; Fig. 4C). Tumors often display a fibrotic stroma, which is characterized by increased collagen deposition as well as altered organization, such as increased collagen density and collagen fiber elongation [21,22]. In the presence of unaltered overall collagen abundance, the observed increased SHG collagen I density score in LN+ patients eludes to a stroma with increased cross-linking and elongated collagen fibers. Collagen III staining within epithelial and stromal compartments was significantly increased in LN+ cases: 22.28 (95% CI 15.93–23.79) versus 16.11 (95% CI 12.65–17.37, $p = 0.006$; Fig. 4D). FN1 staining was also significantly increased in LN+ patients: 26.36 (95% CI 20.32–36.94) versus 17.93 (95% CI 10.83–24.23, $p = 0.001$; Fig. 4E). Despite their association with nodal status, none of these ECM factors were found to be associated with the level of stromal CD4 effector cell density (Supplementary Table 6).

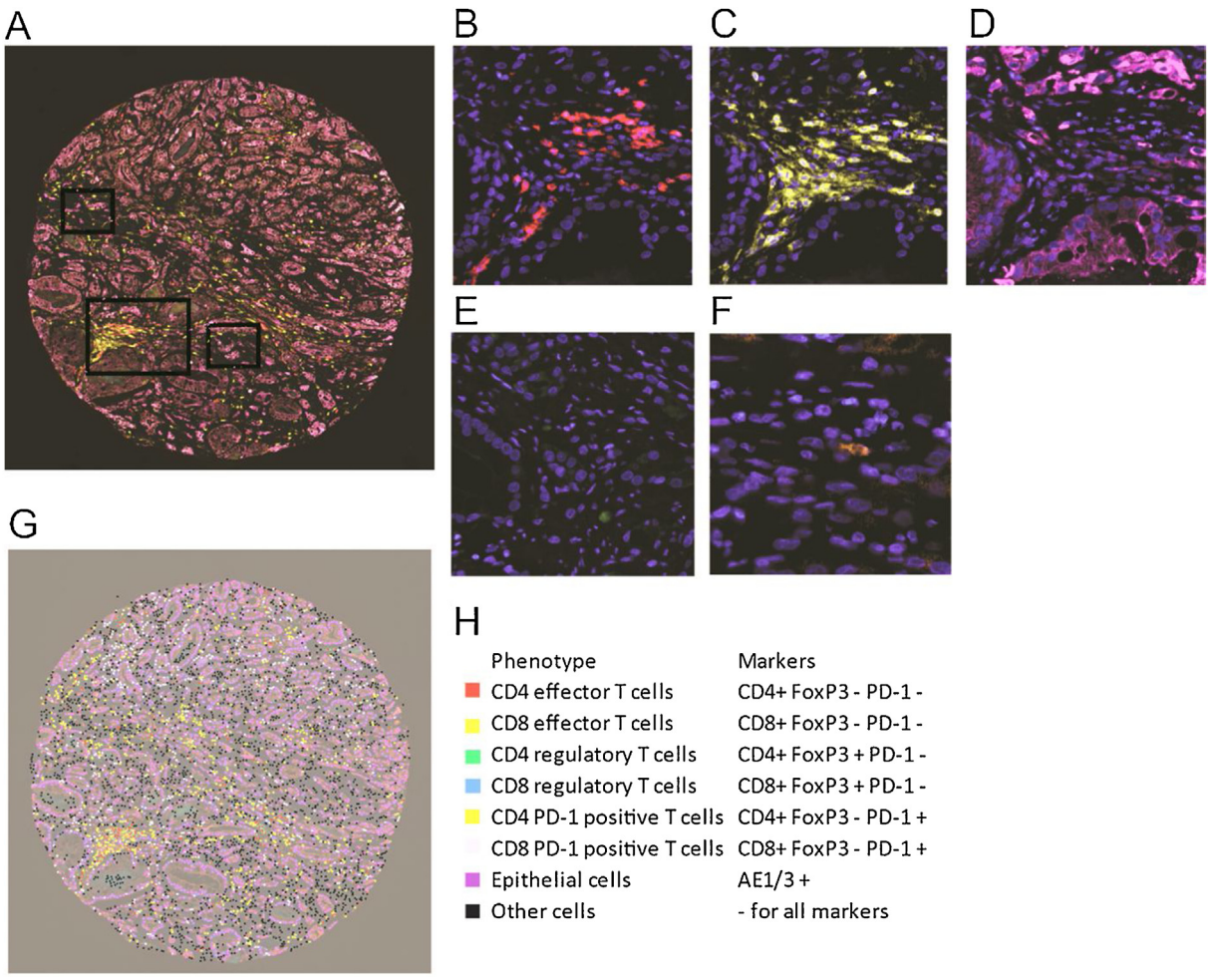

Fig. 2 – Application of a lymphocytic T-cell multiplex immunofluorescence panel in prostate cancer primary tumors. (A) A spectrally unmixed prostate cancer core stained with the lymphocytic T cell panel (panel 2). Enlarged subsections of the core highlighted in Figure 2A, showing each markers of the composite image individually after spectral unmixing, together with DAPI nuclear marker (blue pseudocolor) and autofluorescence signal (black pseudocolor): (B) CD8 (labeled with Opal 520, red pseudocolor), (C) CD4 (labeled with Opal 570, yellow pseudocolor), (D) AE1/3 Pancytokeratin (labeled with Opal 620, magenta pseudocolor), (E) FoxP3 (labeled with Opal 690, green pseudocolor), (F) PD-1 (labeled with Opal 650, orange pseudocolor), and (G) Cell phenotype map of the same core as in Figure 2A identifying the cell populations defined by the individual markers of the multiplex immunofluorescence stain. (H) Summary of each defined cell phenotype (pseudocolor used for visualization and associated markers). (Images shown were obtained at 10× magnification.)

3.5. Validating tumor immune signature associated with LN+ disease

A summary of the immune cell densities for the validation cohort (184 informative cases; Supplementary Table 7), stratified by nodal status, is presented in Supplementary Table 8. Consistent with the findings from the discovery TMA, stromal CD4 effector T-cell populations were significantly decreased in LN+ patients (51.8 vs 100.5 cells/mm^2, $p < 0.001$; Supplementary Table 8). Insignificant trends of reduced tumor (epithelial) CD8 cytotoxic T cells and (epithelial or stromal) M1-like macrophage infiltration were observed between patients with and without nodal disease (Supplementary Table 8).

3.6. Stromal CD4 effector cells predicted presence of LN spread

A crucial question was whether different immune cell infiltrates could be used as predictive biomarkers of LN invasion. Since stromal CD4 effector T cells were identified as the immune cell population reproducibly associated with the status of nodal involvement, we formally tested whether stromal CD4 effector T-cell infiltrates independently predict the presence of pelvic nodal disease. We performed multivariate regression analyses on data from the discovery cohort, including standard of care clinicopathological factors (namely pT stage, Gleason score from RP, peak preoperative PSA level, and percentage of positive cores) currently used to predict the presence of regional LN metastasis according to the Briganti nomogram [23]. Stromal CD4 effector T-cell density remained an independent predictor of LN spread (odds ratio [OR] = 0.15, $p = 0.004$; Table 3). Similarly, based on data from the validation cohort, stromal CD4 effector T-cell density remains a significant independent predictor of LN metastasis (OR = 0.26, $p < 0.001$; Table 3).

Table 2 – Comparisons of intraepithelial and stromal immune cell densities (cells/mm^2) in patients with and without lymph node metastasis

Immune cell densities, cells/mm^2 (95% CI)	All (N = 94)	Lymph node metastasis		
		LN– = 44	LN+ = 50	p value
Epithelium				
M1-like macrophages	**83**	**20.64 (17.07–27.45)**	**16.38 (11.01–21.15)**	**0.046**
M2-like macrophages	83	18.46 (11.49–24.9)	16.2 (11.98–31.94)	0.895
B cells	83	2.81 (1.41–8.29)	1.7 (0.84–4.2)	0.205
CD4 effector T cells	66	23 (13.3–32.9)	18 (11.8–22)	0.093
CD4 regulatory T cells	66	3.25 (1–6.2)	1.5 (0–4.2)	0.159
CD4 PD-1–positive T cells	57	8.02 (0–18.7)	16.2 (5.87–21.7)	0.19
CD8 effector T cells	**66**	**12.6 (6.5–21)**	**1.8(0.68–5.7)**	**0.001**
CD8 regulatory T cell	66	3.8 (0.41–5.69)	2.2 (0.5–4.8)	0.772
CD8 PD-1–positive T cells	66	5.3 (0–9.4)	0 (0–6.82)	0.277
Stroma				
M1-like macrophages	**83**	**64.04 (39.11–89.31)**	**45.03 (39.7–55.3)**	**0.047**
M2-like macrophages	83	65.32 (53.91–76.92)	73.83 (54.69–83.85)	0.7
B cells	83	8.9 (5.27–23.53)	7.05 (4.27–11.51)	0.193
CD4 effector T cells	**66**	**91.35 (55.41–154.1)**	**32.5 (14.1–70.61)**	**<0.001**
CD4 regulatory T cells	66	4.65 (1.6–7.94)	4.71 (3.6–5.4)	0.971
CD4 PD-1–positive T cells	66	7.74 (0–16.2)	8.73 (1.8–13.3)	0.597
CD8 effector T cells	**66**	**40.63 (28.1–95.46)**	**22.7 (11.5–31.38)**	**0.008**
CD8 regulatory T cells	66	0.56 (0.29–1.9)	0.51 (0.31–1.7)	0.9
CD8 PD-1–positive T cells	66	8.1 (2.9–16.3)	4.66 (0.7–7.9)	0.06

CI = confidence interval; LN = lymph node.
Mann-Whitney test was used for all statistical calculations. Significant data on immune infiltrates are presented in bold.

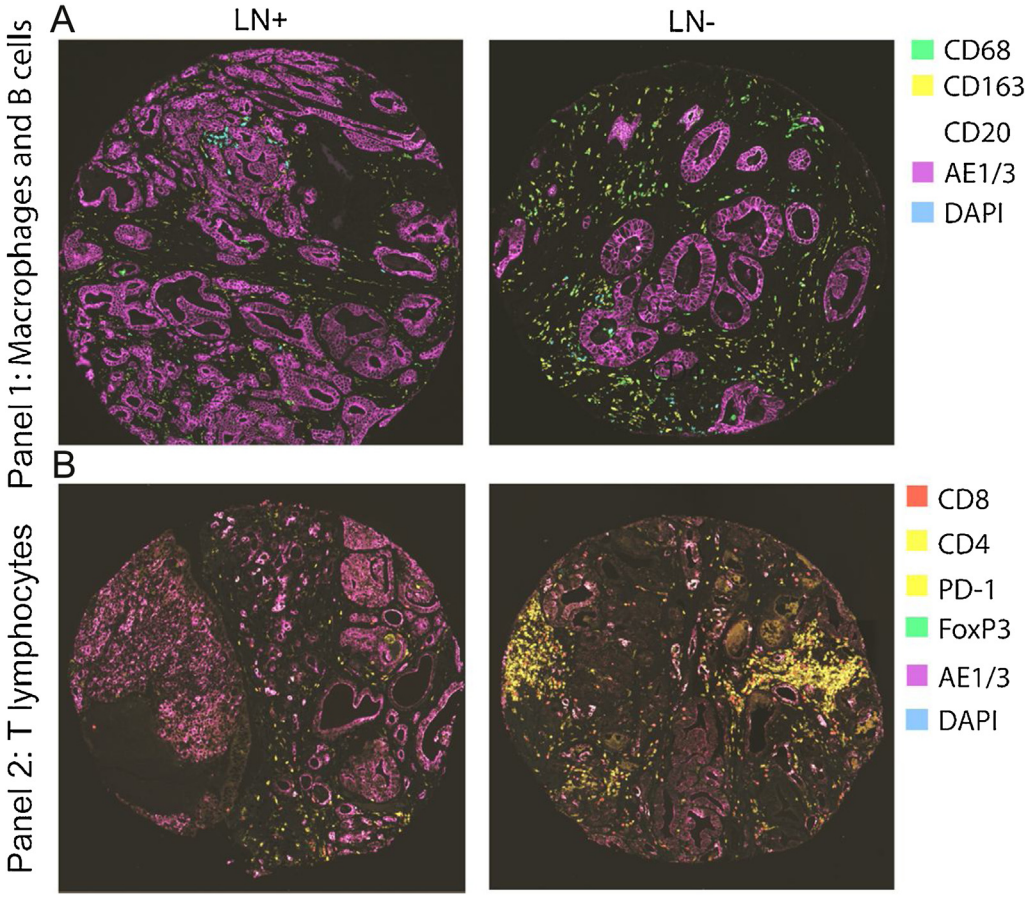

Fig. 3 – Representative multiplex immunofluorescence images showing reduced immune cell infiltration in patients with (LN+; left) versus patients without (LN–; right) LN metastasis. Images are spectrally unmixed for (A) panel 1: macrophage and B cell and (B) panel 2: T lymphocyte. LN = lymph node.

A

Gene	Full gene name	Fold Change LN + vs LN -	adjusted p value
Upregulated			
CXCL14	C-X-C Motif Chemokine Ligand 14	2.56	<0.001
ISG15	Interferon-stimulated gene 15	2.14	<0.001
IFI6	Interferon Alpha Inducible Protein 6	1.85	0.025
FAPa	Fibroblast Activation Protein Alpha	1.83	<0.001
LYZ	Lysozyme	1.8	0.016
COL1A1	**Collagen Type I Alpha 1 Chain**	**1.73**	**0.016**
FCGR3A_3B	Fc Fragment Of IgG Receptor IIIa	1.7	<0.001
FN1	**Fibronectin 1**	**1.68**	**0.039**
OAS3	2'-5'-Oligoadenylate Synthetase 3	1.62	0.003
COL3A1	**Collagen Type III Alpha 1 Chain**	**1.6**	**0.025**
LAPTM5	Lysosomal Protein Transmembrane 5	1.58	0.015
HLA-DRA	Major Histocompatibility Complex, Class II, DR Alpha	1.54	0.041
FCGR2A_2C	Fc Fragment Of IgG Receptor IIa	1.53	0.002
IGFBP3	Insulin growth factor binding pr 3	1.52	0.043
TYROBP	TYRO Protein Tyrosine Kinase Binding Protein	1.51	0.009
Downregulated			
PAGE3	Prostate-Associated Gene 3 Protein	-1.69	0.045
CD244	CD244 Molecule	-1.68	0.048
RND2	Rho Family GTPase 2	-1.65	0.025
TCL1B	Activation Induced Cytidine Deaminase	-1.55	0.048

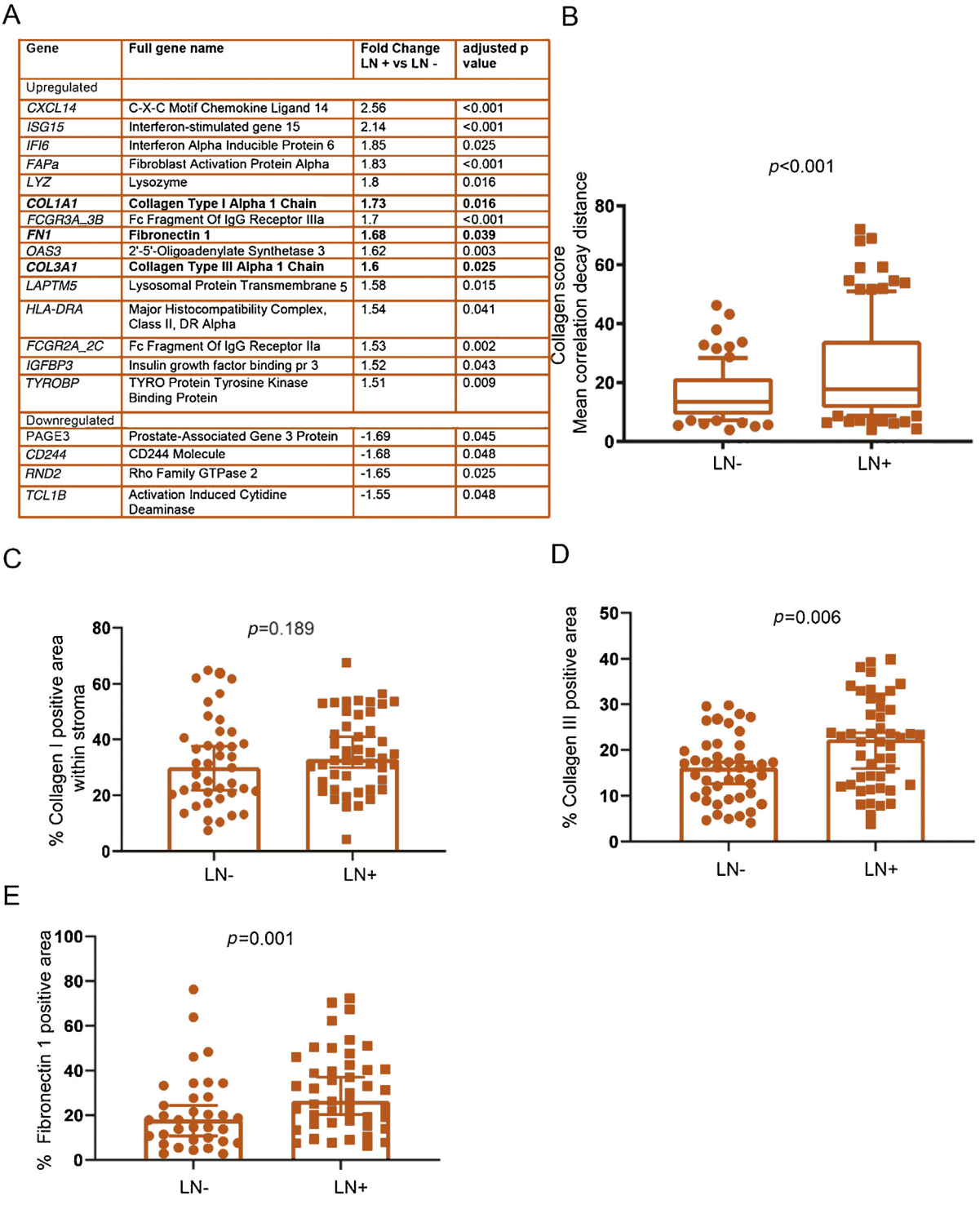

Fig. 4 – Extracellular matrix components with the primary tumors are increased and disorganized in patients with lymph node metastasis. (A) Differentially expressed genes in patients with and without lymph node metastasis revealed upregulation of core ECM components (namely collagen I/*COL1A1*, collagen III/*COL3A1*, and fibronectin 1/*FN1*) in patients with LN metastasis (fold change >1.5, adjusted $p < 0.05$). (B) Mean decay distance of the second harmonic generation (SHG) signal emitted by fibrillar collagen I. Mean decay distance is represented by boxplots showing the second and third quartiles of the data, with the whiskers indicating the maximum and minimum data points for LN– ($n = 89$) and LN+ ($n = 113$) cores. Outliers are shown by individual data points. (C) Percentage of stroma positive for collagen I staining is presented as median with 95% CI in LN– ($n = 41$) and LN+ ($n = 46$) patients. Collagen I was restricted to stroma, and in order to avoid confounding from the relative epithelial/stromal ratio in each core, we quantified the presence of collagen I within the stromal compartment only. (D) Percentage (%) of collagen III staining is presented as median with 95% CI in LN– ($n = 44$) and LN+ ($n = 47$) patients. Lymph node–positive tumors had higher collagen III immunoreactivity. (E) Percentage of FN1 staining is presented as median with 95% CI in LN– ($n = 34$) and LN+ ($n = 45$) patients. Two-tailed Mann-Whitney test was used for all statistical comparisons. CI = confidence interval; ECM = extracellular matrix; LN = lymph node.

Table 3 – Multivariate regression analysis of stromal CD4 effector T cells with standard of care clinicopathological factors commonly used for the prediction of nodal metastasis

	OR	95% CI	*p* value
Discovery cohort			
pT stage	2.96	0.72–12.12	0.131
Gleason score	1.05	0.24–4.57	0.944
Peak preop PSA	0.99	0.94–1.03	0.719
Percentage of positive cores	1.01	0.99–1.03	0.175
Number of lymph nodes excised	0.95	0.87–1.03	0.254
High stromal CD4 effector T cells	**0.15**	**0.04–0.53**	**0.004**
Validation TMA			
pT stage	2.49	1.17–5.27	0.017
Gleason score	3.74	1.48–9.44	0.005
Peak preop PSA	1.04	1.02–1.5	<0.001
High stromal CD4 effector T cells	**0.26**	**0.12–0.54**	<**0.001**

CI = confidence interval; OR = odds ratio; PSA = prostate-specific antigen; TMA = tissue microarray.
For pT stage, the reference was pT2 versus pT3–4. For Gleason score, the reference was Gleason score 7 versus Gleason score >7.
In the discovery cohort, high density of stromal CD4 effector T cells (upper two tertiles) was an independent predictor of lymph node metastasis. In the validation cohort, high density of stromal CD4 effector T cells (upper tertile) was an independent predictor of lymph node metastasis. Significant data on immune infiltrates are presented in bold.

3.7. *Increased stromal CD4 effector cells were associated with improved survival*

During tumor progression, pelvic LNs are common sites for metastases. All cancer staging systems, including the TNM staging system for PCa, assess the presence of LN involvement as part of clinical evaluation of patient prognosis [24]. Applying Youden's Index analysis, we determined the threshold CD4 effector T-cell density in the validation cohort to be 53.15 cells/mm^2, which was applied to the discovery and validation cohorts as a cutoff to define the CD4 effector status in a multivariate generalized linear model in predicting nodal status: discovery cohort (n = 94), p = 0.015; validation cohort (n = 182), p = 0.0003. An ROC analysis showed increased area under the curve (AUC) with the addition of CD4 effector T-cell status, although not reaching statistical significance by Delong's test (discovery cohort: AUC = 60.2 vs 70.6, p = 0.13; validation cohort: AUC = 78.1 vs 80.5, p = 0.32; Fig. 5A and B). Decision curve analysis was then performed showing the standardized net benefit for risk thresholds, suggesting that the addition of CD4 effector cell status may improve the performance in detecting nodal metastasis (solid green vs solid red line in Fig. 5C), with the greatest benefit versus risk (signified by the largest difference between true positive and false positive findings) in patients with medium risk (risk threshold range of 0.4–0.6; Fig. 5D). In addition, analysis of the overall positive and the true positive for node-positive disease also suggested the usefulness of CD4 effector cell status as a marker in the medium- to high-risk range (risk threshold >0.4; Fig. 5E). Consistent with the literature, the presence of nodal metastasis was associated with less favorable relapse-free survival in the validation cohort (Fig. 5F). Applying tumor stromal CD4 effector T-cell density to stratify patients in the validation cohort, patients with reduced CD4 effector T cells were found to have poorer relapse-free survival outcome (Cox's proportional hazards model p = 0.03, hazard ratio = 1.49, n = 168, 132 events; Fig. 5G).

4. Discussion

To the best of our knowledge, this is the first study to have carried out a comprehensive analysis of the tumor immune infiltrates and the tumor transcriptome to investigate for potential associations with PCa pelvic nodal metastasis. There has been significant progress in gene expression approaches to PCa prognostication [25]. However, there has been little advancement in protein-based approaches, even though dysregulated protein expression is more directly linked with the phenotype of invasive PCa. We propose that the addition of stromal CD4 effector T-cell immune cell density of intermediate- and high-risk tumors can improve the current algorithms of nodal metastasis prediction tools such as the Briganti nomogram [23]. This could easily be implemented at the diagnostic biopsy setting and potentially spare patients from the unnecessary side effects of LN dissection. Similarly, a tumor immune signature informed decision on whole pelvic radiation can be based on the likelihood of nodal disease. While the adoption of quantitative mIF in the clinical setting may be challenging, future optimization of a chromogenic IHC assay warrants assessment in diagnostic prostate needle biopsy cores.

For the first time, we show that stromal CD4 effector T-cell infiltration significantly correlates with LN metastasis in PCa. Even though CD8 T-cell infiltration is generally accepted as a tumor suppressive immune subpopulation, CD4 effector T cells have been highlighted as key players of the immune response [26]. Effector helper T cells are essential for the initiation and maintenance of anticancer immune responses. They are known to induce the transformation of cytotoxic T cells into long-lived functional effector cells [27].

Impaired immune infiltrates in progressing tumors may result from the lack of migration cues mediated by chemokines required for T-cell receptor stimulation. Data from our transcriptomic analysis on chemokine expression was not conclusive, with three chemokines found to be

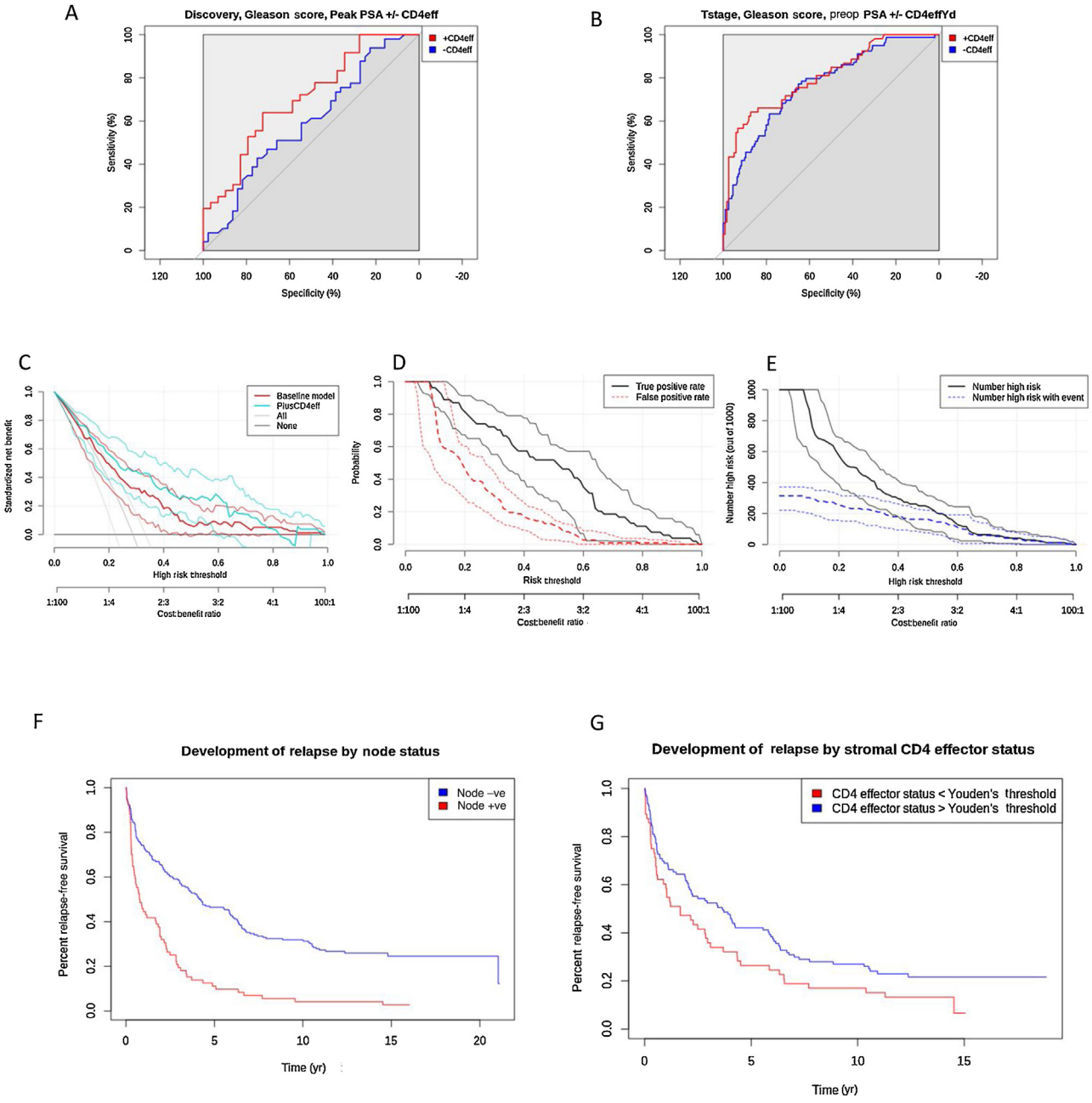

Fig. 5 – Clinical impact of stromal CD4 effector T cells in lymph node metastasis and survival. ROC curves of multivariate generalized linear model (GLM) predictions demonstrating the positive effect of adding tumor stromal CD4 effector T-cell density status to standard of care clinicopathological factors (T stage, Gleason grade, and preoperative PSA) in predicting lymph node metastasis in the (A) discovery and (B) validation cohorts. (C–E) Decision curve analysis for two risk models of lymph node metastasis for validation cohort (generated using R package rmda). (C) The vertical axis showing standardized net benefit and the two horizontal axes showing the correspondence between risk threshold and cost:benefit ratio of the use of CD effector status to predict lymph node metastasis. Baseline model (thick red line) includes standard of care clinicopathological factors (T stage, Gleason grade, and preoperative PSA). Thick blue line signifies the addition of CD4 effector status (95% confidence intervals [CIs] by bootstrapping are represented by thin lines of the respective colors). (D) True positive (thick black line) and false positive (dotted red line) rates as functions of the risk threshold for the CD4 effector status risk model (95% CI thin lines). (E) Clinical impact curve for the risk model including CD4 effector status. Of 1000 patients, the black solid line shows the total number of patients deemed to be at a high risk for lymph node metastasis by low CD4 effector status for each risk threshold. The blue dashed line shows the number of patients found to be true positive with lymph node metastasis (95% CI thin lines). Kaplan-Meier curves of patients in the validation cohort with PCa showed shorter relapse-free survival among (F) those positive for nodal metastasis (red = node + ve; blue = node –ve) and (G) those with a lower density of effector CD4 T cells in the stromal compartment (red = lower, blue = higher)). Cox's proportional hazards model was used for statistical comparisons. Stromal CD4 effector T-cell density values were dichotomized according to the CD4 effector T-cell density threshold cutoff at $\geq$54.6 cells/mm^2 (red line) or $<$54.6 cells/mm^2 (blue line), as determined by Youden's Index analysis. PSA = prostate-specific antigen; ROC = receiver operator characteristic.

significantly upregulated (Fig. 4A). Upregulated *ISG15* and *AFI6* expression in tumors with nodal disease is consistent with increased tumorigenesis, but upregulated *CXCL14* levels were suggested to suppress cancer invasion. Instead, core ECM molecules were increased at both mRNA and protein levels in LN+ patients. Enhanced ECM deposition and remodeling results in a more disorganized and fibrotic stroma in LN+ patients. Tumor-associated fibrosis is a well-established regulator of tumor progression but can also be a critical regulator of immune surveillance [28–31]. High collagen density may function as a physical barrier for T-cell infiltration in pancreatic ductal adenocarcinoma and was able to abolish completely chemokine-guided movement [30]. Our results are consistent with the notion that a remodeled and denser ECM may hinder effector T-cell infiltration in PCa in the context of regional LN tumor infiltration.

Despite the overall validity of the data produced by multispectral imaging, some limitations should be mentioned. There was some degree of crosstalk between fluorophores with overlapping emission spectra, that is, FoxP3 Opal 690/PD-1 Opal 650 and AE1/3 Opal 620. This problem was circumvented by phenotyping cells based on their cellular morphology as well as marker expression. Finally, our study suffers the key risk of undersampling due to tumor heterogeneity. Nonetheless, the fact that our immune signature was validated in an independent cohort provides confidence to our working model.

While the transcriptomic analysis was performed on prostate biopsy materials, we have carefully selected the biopsy cores from the respective index lesions that were incorporated in the TMA; thus data from transcriptomic analysis are relevant to observations from the mIF experiment. Furthermore, candidate genes identified to be differentially expressed were further studied at the protein level (including the level of stromal collagen or fibronectin present) using the same TMA studied for mIF. In this way, data on candidate markers within the ECM can be interpreted with confidence to tumor immune infiltrates. To date, no clear causality between ECM density and immune exclusion has been established in PCa. Indeed, we did not find a clear relationship between expression of ECM proteins and CD4 effector status. The efficacy of single-agent immunotherapies in PCa have so far been unsuccessful [32]. Our data suggest that stratification of PCa tumors based on tumor microenvironment warrants further investigations. Finally, the discovery cohort was selected to include similar number of patients with and without nodal metastasis. As a result of such biased nature, we have not included this cohort in patient outcome analysis. Future evaluation of CD4 effector cell density in additional clinical cohorts is required.

5. Conclusions

Decreased T-cell infiltrates in the primary tumor (particularly CD4 effector cells) are associated with a higher risk of LN metastasis. Future evaluation of CD4-based assays on PCa diagnostic biopsy materials may improve selection of at-risk patients for treatment of LN metastasis.

Author contributions: Hing Y. Leung had full access to all the data in the study and takes responsibility for the integrity of the data and the accuracy of the data analysis.

Study concept and design: Ntala, Salmond, Carlin, Le Quesne, Blomme, Goodyear, Kruithof-de Julio, Thalmann, Jamaspishvili, Berman, Roberts, Ahmad, Leung.
Acquisition of data: Ntala, Salmond, Officer, Teodosio, McGhee, Powley, Jamaspishvili, Berman, Leung.
Analysis and interpretation of data: Ntala, Salji, Salmond, Officer, Teodosio, McGhee, Powley, Jamaspishvili, Berman, Leung.
Drafting of the manuscript: Ntala, Salji, Blomme, Le Quesne, Goodyear, Leung.
Critical revision of the manuscript for important intellectual content: Carlin, Salmond, Kruithof-de Julio, Thalmann, Jamaspishvili, Berman, Roberts, Ahmad.
Statistical analysis: Ntala, Salji.
Obtaining funding: Ntala, Carlin, Le Quesne, Thalmann, Berman, Leung.
Administrative, technical, or material support: None.
Supervision: None.
Other: None.

Financial disclosures: Hing Y. Leung certifies that all conflicts of interest, including specific financial interests and relationships and affiliations relevant to the subject matter or materials discussed in the manuscript (eg, employment/affiliation, grants or funding, consultancies, honoraria, stock ownership or options, expert testimony, royalties, or patents filed, received, or pending), are the following: None.

Funding/Support and role of the sponsor: CRUK (A22904, A17196, A19661, A23983).

Appendix A. Supplementary data

Supplementary material related to this article can be found, in the online version, at doi:https://doi.org/10.1016/j.euros.2021.05.001.

References

[1] Rawla P. Epidemiology of prostate cancer. World J Oncol 2019;10:63–89.
[2] Angell H, Galon J. From the immune contexture to the Immunoscore: the role of prognostic and predictive immune markers in cancer. Curr Opin Immunol 2013;25:261–7.
[3] Galon J, Mlecnik B, Bindea G, et al. Towards the introduction of the' Immunoscore' in the classification of malignant tumours. J Pathol 2014;232:199–209.
[4] Mezheyeuski A, Bergsland CH, Backman M, et al. Multispectral imaging for quantitative and compartment-specific immune infiltrates reveals distinct immune profiles that classify lung cancer patients. J Pathol 2018;244:421–31.
[5] Carstens JL, Correa de Sampaio P, Yang D, et al. Spatial computation of intratumoral T cells correlates with survival of patients with pancreatic cancer. Nat Commun 2017;8:15095.
[6] Brown JR, Wimberly H, Lannin DR, Nixon C, Rimm DL, Bossuyt V. Multiplexed quantitative analysis of CD3, CD8, and CD20 predicts response to neoadjuvant chemotherapy in breast cancer. Clin Cancer Res 2014;20:5995–6005.

[7] Geissler K, Fornara P, Lautenschlager C, Holzhausen HJ, Seliger B, Riemann D. Immune signature of tumor infiltrating immune cells in renal cancer. Oncoimmunology 2015;4:e985082.
[8] Fridman WH, Pagès F, Sautès-Fridman C, Galon J. The immune contexture in human tumours: impact on clinical outcome. Nat Rev Cancer 2012;12:298–306.
[9] Huang W, Hennrick K, Drew S. A colorful future of quantitative pathology: validation of Vectra technology using chromogenic multiplexed immunohistochemistry and prostate tissue microarrays. Hum Pathol 2013;44:29–38.
[10] Toth ZE, Mezey E. Simultaneous visualization of multiple antigens with tyramide signal amplification using antibodies from the same species. J Histochem Cytochem 2007;55:545–54.
[11] Stack EC, Wang C, Roman KA, Hoyt CC. Multiplexed immunohistochemistry, imaging, and quantitation: a review, with an assessment of tyramide signal amplification, multispectral imaging and multiplex analysis. Methods 2014;70:46–58.
[12] Gollapudi K, Galet C, Grogan T, et al. Association between tumor-associated macrophage infiltration, high grade prostate cancer, and biochemical recurrence after radical prostatectomy. Am J Cancer Res 2013;3:523–9.
[13] Cao J, Liu J, Xu R, Zhu X, Zhao X, Qian BZ. Prognostic role of tumour-associated macrophages and macrophage scavenger receptor 1 in prostate cancer: a systematic review and meta-analysis. Oncotarget 2017;8:83261–9.
[14] Ness N, Andersen S, Valkov A, et al. Infiltration of CD8+ lymphocytes is an independent prognostic factor of biochemical failure-free survival in prostate cancer. Prostate 2014;74:1452–61.
[15] Flammiger A, Bayer F, Cirugeda-Kuhnert A, et al. Intratumoral T but not B lymphocytes are related to clinical outcome in prostate cancer. Acta Pathol Microbiol Immunol Scand 2012;120:901–8.
[16] McArdle PA, Canna K, McMillan DC, McNicol AM, Campbell R, Underwood MA. The relationship between T-lymphocyte subset infiltration and survival in patients with prostate cancer. Br J Cancer 2004;91:541–3.
[17] Gopalan A, Leversha MA, Satagopan JM, et al. TMPRSS2-ERG gene fusion is not associated with outcome in patients treated by prostatectomy. Cancer Res 2009;69:1400–6.
[18] Demichelis F, Fall K, Perner S, et al. TMPRSS2:ERG gene fusion associated with lethal prostate cancer in a watchful waiting cohort. Oncogene 2007;26:4596–9.
[19] Lotan TL, Gurel B, Sutcliffe S, et al. PTEN protein loss by immunostaining: analytic validation and prognostic indicator for a high risk surgical cohort of prostate cancer patients. Clin Cancer Res 2011;17:6563–73.
[20] Lotan TL, Wei W, Morais CL, et al. PTEN loss as determined by clinical-grade immunohistochemistry assay is associated with worse recurrence-free survival in prostate cancer. Eur Urol Focus 2016;2:180–8.
[21] Lu P, Weaver VM, Werb Z. The extracellular matrix: a dynamic niche in cancer progression. J Cell Biol 2012;196:395–406.
[22] Peranzoni E, Rivas-Caicedo A, Bougherara H, Salmon H, Donnadieu E. Positive and negative influence of the matrix architecture on antitumor immune surveillance. Cell Mol Life Sci 2013;70:4431–48.
[23] Briganti A, Larcher A, Abdollah F, et al. Updated nomogram predicting lymph node invasion in patients with prostate cancer undergoing extended pelvic lymph node dissection: the essential importance of percentage of positive cores. Eur Urol 2012;61:480–7.
[24] Amin MB, Edge S, Greene F, et al., editors.AJCC cancer staging manual. ed. 8. Springer; 2017.
[25] Peng Z, Skoog L, Hellborg H, et al. An expression signature at diagnosis to estimate prostate cancer patients' overall survival. Prostate Cancer Prostatic Dis 2014;17:81–90.
[26] Wakabayashi O, Yamazaki K, Oizumi S, et al. CD4+ T cells in cancer stroma, not CD8+ T cells in cancer cell nests, are associated with favorable prognosis in human non-small cell lung cancers. Cancer Sci 2003;94:1003–9.
[27] Bevan MJ. Helping the CD8(+) T-cell response. Nat Rev Immunol 2004;4:595–602.
[28] Jiang H, Hegde S, DeNardo DG. Tumor-associated fibrosis as a regulator of tumor immunity and response to immunotherapy. Cancer Immunol Immunother 2017;66:1037–48.
[29] Salmon H, Franciszkiewicz K, Damotte D, et al. Matrix architecture defines the preferential localization and migration of T cells into the stroma of human lung tumors. J Clin Invest 2012;122:899–910.
[30] Hartmann N, Giese NA, Giese T, et al. Prevailing role of contact guidance in intrastromal T-cell trapping in human pancreatic cancer. Clin Cancer Res 2014;20:3422–33.
[31] Bougherara H, Mansuet-Lupo A, Alifano M, et al. Real-time imaging of resident T cells in human lung and ovarian carcinomas reveals how different tumor microenvironments control T lymphocyte migration. Front Immunol 2015;6:500.
[32] Topalian SL, Hodi FS, Brahmer JR, et al. Safety, activity, and immune correlates of anti-PD-1 antibody in cancer. N Engl J Med 2012;366:2443–54.